Title: Numerical modeling of the interaction of pressurized large diameter gas buried pipelines with normal fault ruptures

Authors: AG Özcebe[1,2]; R Paolucci[3]; S Mariani[4]

Abstract:

There is a growing attention towards the seismic response of large diameter pipelines, owing to the potential adverse impact on economy and civilized life of a structural collapse under earthquake effects, such as strong ground shaking, and other earthquake related effects such as fault rupture, landsliding and liquefaction. The intersection of a fault rupture with a pipeline is of special concern, because the safety verification is affected by significant uncertainties in the loading condition, related to the unknown exact location where the fault offset may occur, the unknown amount of the offset itself, as well as the intersection angle of the fault rupture with the pipe axis. Besides, the inherent analytical/numerical complexity of the problem may require 3D finite element models with non-linear constitutive laws and large deformations.

In this paper a summary is presented of a comprehensive set of 3D numerical simulations of the interaction of a large diameter gas pipeline with a normal fault rupture, with the main objectives of: 1) throwing light on the pipeline performance under increasing levels of fault offset, including cross-sectional buckling and ovalization; 2) providing a parametric set of results, including the variability of the fault-pipe intersection angles, of the mechanical properties of the pipe-soil interface, as well as of the operating conditions, in terms of internal gas pressure and temperature variations.

Keywords: fault-soil-pipeline interaction, 3D finite element modeling, performance based seismic design

Affiliations:

1. Department of Civil and Environmental Engineering, Politecnico di Milano, Milano, Italy. e-mail: **aliguney.ozcebe@polimi.it** (Corresponding author)
2. European Centre for Training and Research in Earthquake Engineering (EUCENTRE), Pavia, Italy.
3. Department of Civil and Environmental Engineering, Politecnico di Milano, Milano, Italy. e-mail: **roberto.paolucci@polimi.it**
4. Department of Civil and Environmental Engineering, Politecnico di Milano, Milano, Italy. e-mail: **stefano.mariani@polimi.it**

1. INTRODUCTION

Seismic response of buried pipelines is mainly governed by the kinematic interaction between soil and structure rather than by inertial actions [7]. On one side, such interaction may induce transient effects, related to straining due to seismic wave propagation. On the other side, permanent effects are related to irreversible ground failure, induced either by lateral spread/vertical settlements as a result of soil liquefaction, or by lateral/oblique displacement as a result of slope instability, or by horizontal/vertical offset due to fault rupture crossing [20].

The experience from past earthquake has shown that, apart from few cases (e.g. [7], [20]) structural failures of pipelines are mainly associated to permanent ground deformations (see, e.g., [9], [31], [33]). Among the latter cases, pipelines are mostly vulnerable to active fault crossings (e.g. [17]) since the strength of the surrounding soil may not reduce significantly as in the liquefaction or landsliding problems, and localized large straining are likely to occur along the pipeline. Several well-known examples of major pipeline failures induced by the interaction with the seismic fault offset are from San Fernando (California, 1971) [19], Manjil (Iran, 1990) [23], Kocaeli (Turkey, 1999) [8], and Chi-Chi (Taiwan, 1999) [16].

Analytical modeling of the buried pipeline-fault interaction problem started with the pioneering work of Newmark and Hall ([10] and [18]), who modeled the pipeline as a cable connected to the soil with nonlinear springs, subsequently refined by Kennedy et al. [14]. These works provided the theoretical support to the 1984 ASCE guidelines [3], which have been for decades the basis for seismic analysis design of pipelines crossing active faults. Subsequently, different researchers provided improvements, in the framework of simplified analytical approaches, such as [12], [13], [22], [27], [28], [29].

Only in the recent years, a substantial experimental activity provided support to the previous analytical approaches. Aside from the shaking table tests performed by Sim et al. [24], who used a special equipment, able to simultaneously simulate the transient vibration due to seismic wave propagation together with the permanent ground displacement caused by fault offset, research work was mostly based on centrifuge tests, such as Abdoun et al. [1], Ha et al. [9], and Xie et al. [32], who verified that the 1984 ASCE guidelines [3] are in good agreement with the experimental results for strike-slip faulting, but they tend to overestimate stiffness and strength of the p-y curves in normal faulting. Centrifuge tests on reverse faulting were reported by Rohjani et al. [23], who noted the dependence of the instability failure modes on the burial depth, moving from general buckling, at shallow depths, to cross-sectional wrinkling, at larger depths.

Both the analytical and experimental works have confirmed the following factors that contribute to the safety of pipelines crossing fault ruptures, (see e.g., Eurocode 8 Part 4 [5]): (i) the depth at which the pipeline is buried should be minimized; (ii) the fault crossing angle of the pipeline should be chosen to promote tensile elongation and reduce compressive strains; (iii) the cross-sectional thickness to diameter ratio should be increased; (iv) the angle of interface friction between the pipeline and the soil should be reduced, by selecting a loose to medium granular soil as backfill material.

Simplified analytical approaches proved to be a very effective tool in understanding the key factors influencing the seismic response of buried pipelines crossing fault ruptures, as well as in determining the threshold values of fault offset to achieve initial pipe yielding, i.e., a damage limit state. However, being typically based on modeling the system as a linear beam on a bed of non-linear springs, they are not suitable to follow extensively the response of the pipeline in the non-linear range, within a performance-based design approach. As a matter of fact, at the relatively large strain levels that are typically prescribed to define the ultimate limit state for a buried pipeline subject to fault rupture, i.e. 3% in tension and 1% in compression according to EC8 Part4, local buckling may occur, which can be reliably predicted only by means of three-dimensional (3D) finite element (FE) numerical approaches.

However, the accurate numerical modeling of this complicated soil-structure interaction problem poses several major numerical difficulties, such as: i) 3D geometry; ii) large deformations; iii) local cross-sectional buckling; iv) Eulerian buckling under compressive fault movement; v) pipe sliding with respect to the surrounding soil; vi) non-linear soil behavior. As a result, such comprehensive numerical analyses are still confined at the research stage, and relatively few examples exist of 3D simulations involving the large-strain non-linear response of all the elements of the problem, i.e., the structure, the soil, and the soil-structure interface (e.g., [11], [21], [22], [25], [26], [33], [34]). In some research works (e.g. [15], [32]), the complexity of the problem is reduced by considering a 3D structural model on a bed of non-linear springs, but, in the latter case, the contribution of interaction among the different components of loading at the soil-foundation interface is lost.

In this paper, we will address, through a 3D numerical finite element approach involving discretization of both soil and pipeline, the response of pressurized buried pipelines subjected to normal fault rupture, which is the common case in Central/Southern Italy, with expected maximum magnitude around 7, corresponding to a maximum expected fault-offset of 1 to 1.5 m [30]. Compared to previous studies on the interaction of normal fault offsets with buried pipelines (e.g. [13]; [32]), the contribution of this paper will mainly focus on the following objectives:

- to highlight the main computational problems to be tackled, especially as regards the longitudinal extent of the model to avoid spurious effects from boundary conditions, that in such computationally demanding 3D numerical simulations may be a critical issue;
- to establish relationships between the pipe performance, measured through standard definitions of serviceability and ultimate limit states, with increasing values of the fault offset;
- to highlight the role, within such relationships, of several parameters, related to geometry (dip angle, fault-pipe intersection angle), to mechanical properties (soil elastic modulus, interface friction angle), and to operating conditions (internal pressure and temperature of the pipe);
- to analyze the changing shape and extension of the plastic zones within the pipe as a function of load conditions;
- to build a set of reliable numerical results to be used as a benchmark to develop and calibrate more simplified approaches usable in the engineering practice.

2. NUMERICAL MODELING

To provide reliable results, the adopted FE approach should properly account on one side for the loading conditions, in terms of operating gas pressure and temperature, of the dead load due to the burying soil layer, as well as of the fault geometry and kinematics, in terms of intersection angle and direction and amount of the fault offset. On the other side, it should properly model the large amount of nonlinear response involved in the pipe and soil responses, including that at their interface.

As a first step, we defined a region including the pipeline and the surrounding soil, the dimensions of which were set in order to avoid disturbances of the boundary conditions on the structural response. This is of concern especially in the longitudinal direction of the pipe, because it should be checked that, in the most heavily strained region close to the fault crossing, the solution is not affected by the numerical boundary conditions which limit the longitudinal extension of the model. As illustrated later, such extension depends on the combination of pipe geometry, non-linear soil response, soil-pipe interaction, fault dip angle and maximum offset, so that it cannot be set a-priori in the analysis, even if its actual impact should be verified a-posteriori.

When symmetry of loading conditions applied along the vertical longitudinal plane holds, only half of the full model was considered in the analysis and discretized.

The loading conditions are applied in two steps. First, the operating conditions in terms of gas pressure and temperature are provided at the inner surface of the pipe, together with the gravity load caused by the soil burying the pipe, leading to a small ovalization of the cross-section. These

loads were applied quasi-statically, and provide the initial conditions from which the fault offset is plugged in the model through progressively increasing values. Due to the prevailing effect of large permanent values of fault offset on the pipeline response, the contribution of transient loading during the seismic excitation, including inertial effects, was disregarded.

The mesh size was set to cope with the two competing requirements of accuracy and minimization of computational costs. Preliminary analyses were run to design an optimum space discretization, to ensure the structural response within the region of interest to be mesh-independent. A finer mesh discretization was selected close to the fault crossing. To avoid numerical locking when large values of the fault offset are applied and large plastic deformations occur, the pipe and the soil were discretized through reduced-integration (with hourglass control) 4-node shell elements and 8-node solid elements, respectively.

Numerical analyses were carried out with the commercial FE code *Abaqus* [6].

3. NUMERICAL RESULTS

3.1. Validation against centrifuge test results of normal fault rupture propagation

Bransby et al. [4] conducted an experimental campaign, based on a centrifuge test carried out to investigate the propagation of a normal fault inside dry, medium dense (D_r=60%), uniform silica sand with the following properties: 50%-passing diameter (d_{50})= 0.3 mm; maximum dry density (ρ_{max})= 1.7 t/m^3; minimum dry density (ρ_{min})= 1.44 t/m^3; internal effective friction angle (ϕ')= 35° and dilation angle (ψ)= 6°. The physical model set-up is shown in Figure 1, with a geometry scaling factor of 115. The main output of the test was the measurement of the displacement field, from which the shear strain field was then computed.

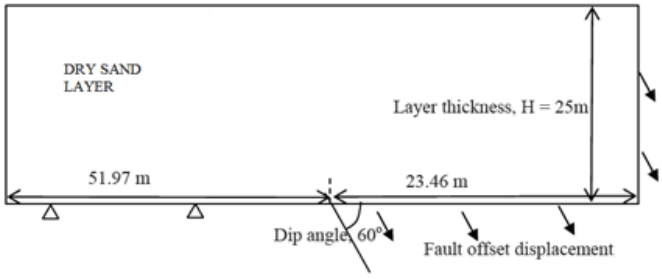

Figure 1. Drawing of the physical model at the prototype scale (after [4])

In the numerical counterpart considered here, still at the prototype scale, plane strain conditions were assumed. The sand response was modelled by an isotropic, elastic perfectly-plastic constitutive law, with equivalent shear modulus (G_{eq}) varying between 20-30 *MPa*; Poisson's ratio ν_s=0.25-0.30, and yielding governed by a Mohr-Coulomb failure condition with non-associated flow rule. The non-uniformity of the gravitational field resulting from the centrifugal acceleration and Earth's gravity acceleration was not taken into consideration. The fault offset was applied as a rigid body motion on the boundaries of the hanging wall (HW) side, as shown in Figure 1. To avoid unrealistically large strains at the interface with the footwall (FW) boundary, a narrow 1 m wide region, in between the HW and the FW, was introduced for the fault offset to gradually increase from zero to its maximum value.

A mesh sensitivity analysis was preliminary carried out, adopting a gradual refinement from a coarser mesh away from the fault crossing (with a characteristic element size of 1.0 m) to a finer one close to the fault (with a characteristic size of 0.25 m). By comparing experimental data and numerical predictions, it was possible to point out that the discretization along the horizontal

direction plays the most important role; accordingly, a structured mesh of quadrilateral elements featuring node spacing of 0.25 m and 0.50 m in the horizontal and vertical directions, respectively, provided a reasonable trade-off between accuracy and computational efficiency.

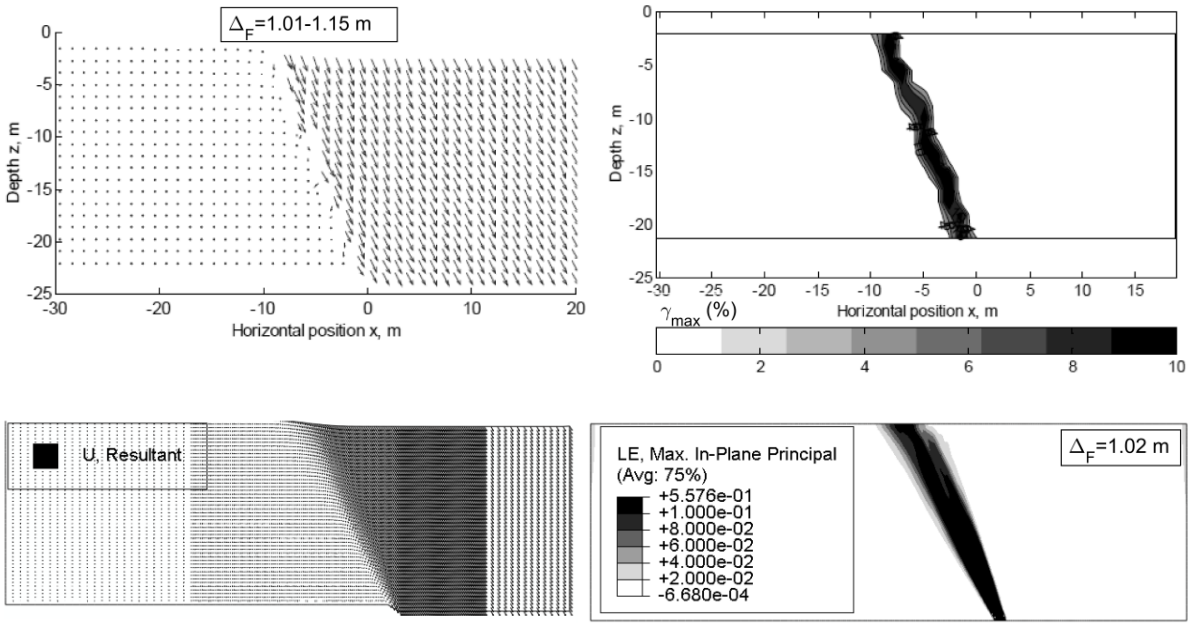

Figure 2. Comparison between experimental (top row, after [4]) and numerical (bottom row) results for the centrifuge model at a fault offset of around 1.0 m. Left column: displacement field; right column: strain field.

In Figure 2, displacement and strain fields obtained with such space discretization are compared with the available experimental data for a fault offset of around 1.2 m, see [4]. The corresponding vertical displacement profiles at a depth of z=0.9 m, are compared in Figure 3. In this figure, numerical results are also illustrated at varying amplitudes Δx of the region across which the fault offset is imposed along the bottom surface of the model, showing a limited dependency of the solution using widths smaller than 1 m.

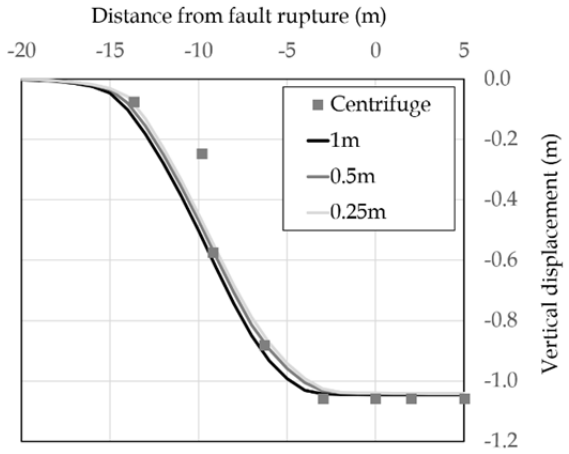

Figure 3. Comparison between experimental (after [4]) and numerical vertical displacement profiles at a depth from surface z=-0.9 m. Results obtained using different amplitudes Δx (=1m, 0.5m, or 0.25m) of the region across which the fault offset is imposed along the bottom surface of the model are compared.

An acceptable agreement between the experimental and numerical displacement profiles was obtained. The formation and inclination of the main shear band in the sand was also satisfactorily predicted, as well as the width of the main shear plane close to fault outcropping, as shown in Fig. 3 by the spreading of the region wherein the vertical displacement jumps. The mismatch between the numerical and experimental datasets may be related to having neglected some effects like:

non-uniform gravitational field at centrifuge conditions, softening of sand, strain localization after yielding, inhomogeneous soil conditions.

It is finally noted that, to pursue the main objectives of this study, i.e., investigating the pipeline performance up to the serviceability and ultimate limit states under increasing values of fault offset, an extreme mesh refinement to capture very localized solutions of soil failure was not considered necessary. A similar compromise between accuracy of the solution and objectives of the analysis is also at the base of the selection of the structural grid size, which is addressed in the next section.

3.2. Case studies of pipe-fault rupture interaction

We start the set of numerical simulations by a benchmark case, where a steep dip angle was associated to the fault plane (δ = 80°), and the fault offset (Δ_F) was increased up to a maximum value of 2 m. The study was carried out by considering first the effect of the fault offset alone (Case 1), then the combined loading by the internal gas pressure and fault offset (p_i=8MPa, Case 2) was applied, and, finally, the operating conditions were completed by considering the additional contribution of the variation of temperature (ΔT = 50°C, Case 3). For all of those cases, the simulation was repeated for lower values of the dip angle (δ=40°-60°), in order to verify its effect not only on the resulting stresses and plastic deformations of the pipe, but also on the geometric modelling assumptions, especially to check whether the length of the modelled portion of the pipeline was sufficiently extended.

In addition to these benchmark numerical simulations, we considered other situations, in order to study the impact of different assumptions, such as the reduced value of the elastic soil modulus (Case 4), the reduced shear strength, both in terms of the friction (φ') and dilatancy (ψ) angles (Case 5), the increase of the soil-pipe interface friction coefficient, to investigate the increased constrain provided by the soil to the pipe movement (Case 6). Finally, in Case 7 we re-considered the benchmark case with operating conditions (Case 3), and checked the effect of a change of plane orientation, i.e., instead of considering the unit vector normal to the fault plane directed as the longitudinal axis of the pipe (α_f = 0°), we selected α_f = 45°. Therefore, only in the latter case symmetry conditions could not be applied. The list of case studies is reported in Table 1.

For all simulations, the geometric characteristics (cross-sectional thickness and diameter) as well the pipeline burial depth were kept constant. A shallowly embedded (H=1.5 m), large diameter (D=1.2 m) gas transmitting pipeline with wall thickness t=0.02 m was modeled. Trench depth (5 m) and width (5.2 m) were chosen consistently with a real case study. Consistently with the former verification stage, the mesh density for the soil is characterized by an average element size in the radial direction of 50 cm. 32 shell elements were used for the spatial discretization of the pipe along its perimeter. By keeping an almost unitary shape ratio for the shell elements, their characteristic size resulted to be around 0.16 m. Although such element size along the longitudinal axis of the pipe is not sufficient to accurately model the evolution of local buckling induced by compressive stress states, it is refined enough to capture the triggering of this ultimate limit state, beyond which our numerical simulations were terminated.

The X60 graded pipe steel was modeled by an elasto-plastic constitutive law, with yielding governed by von-Mises law (f_y=450 MPa), with associated flow rule, and featuring a slight isotropic hardening (r=0.002). The soil was instead assumed to display an elastic, perfectly-plastic response governed by Mohr-Coulomb yield condition, with non-associated flow rule. Further details of the numerical mesh along the cross-sectional plane and of the prescribed material properties are shown in Figure 4.

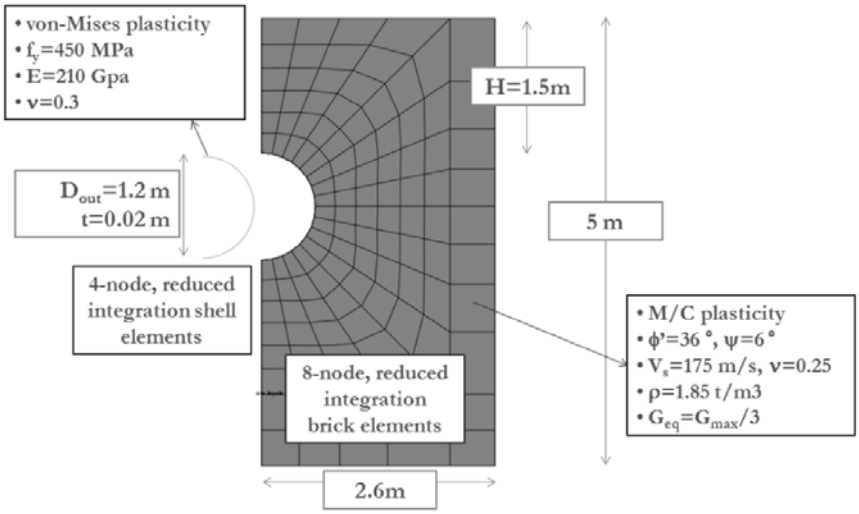

Figure 4. Finite element mesh in the cross-sectional plane and material properties for the benchmark model.

A preliminary investigation was made to determine the optimum longitudinal size of the numerical model, depending on the combined effect of fault offset, dip angle and mechanical soil properties. Eventually, for a single numerical model to be investigated, a conservative value *L*=2000 m was chosen for all case studies. As shown in Figure 5, the density of the mesh was gradually decreased for increasing distance from the fault rupture, after verification of the mesh independence of the numerical results.

Similar to the validation example of Section 3.1, boundary conditions to model the fault slip were applied as follows. For the soil body: (i) the whole outer surface (except for the top) of the FW part was fixed in their outward normal directions and for bottom surface also horizontal fixity is provided, (ii) bottom and vertical planes of the HW part were moved with an increased value of displacement, and (iii) longitudinal sides of HW were fixed along their outward normal directions throughout the longitudinal length of the model *L* ~~all along 2000 m~~. For the pipe elements: (iv) pipe cross-section on the extreme FW side was restrained along the pipe longitudinal direction, (v) pipe cross-section on the extreme HW side was moved with an increased value of displacement (as in (ii)), and (vi) restraints according to symmetry conditions were provided at the symmetry plane, all along L ~~2000 m~~. In Figure 6, in-plane boundary conditions (i.e. (i), (ii), (iv), (v)) are shown.

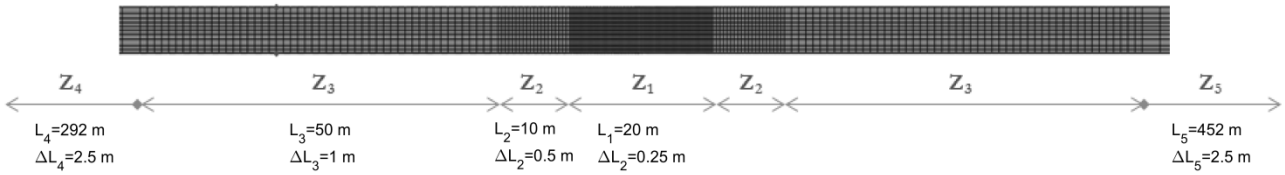

Figure 5. Finite element mesh along the longitudinal direction for the benchmark case.

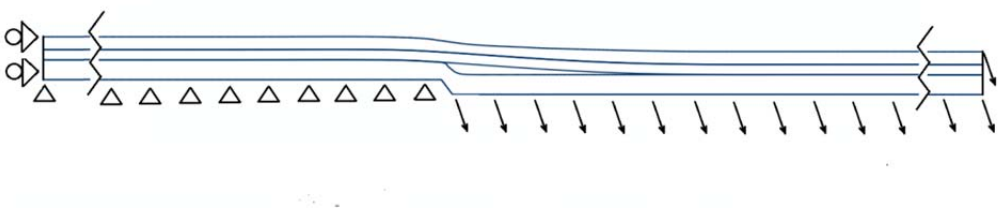

Figure 6. Boundary conditions at the second stage of the analysis (after application of operating loading conditions), for the quasi-static application of fault offset. Out-of-plane boundary conditions are not shown.

The soil and pipe elements are connected with zero length interface (contact) elements, for which no normal deformation is permitted, while shear deformations are controlled by the shear strength of the interface. The latter is taken as 2/3 of the soil effective friction angle, in agreement with ALA Guidelines [2].

Table 1. List of case studies with the parameters considered in the sensitivity analysis. Soil parameters: shear wave velocity (V_s), mass density (ρ), equivalent linear shear modulus (G_{eq}), soil Poisson's ratio (ν), internal effective friction angle (φ'), dilation angle (ψ), effective cohesion (c') Structure parameters: Modulus of elasticity for steel (E_s), steel Poisson's ratio (ν_s), yield strength of steel (f_y), bilinear hardening ratio (r).

#	Soil	Structure	Interface	Fault Angle	Operating conditions	Aim
1	V_s=175 m/s, ρ=1.85 t/m^3 G_{eq}=0.33G_{max}, ν=0.25, ϕ'=36°, ψ'=6°, c'=0.1 kPa	E_s=210 GPa, ν_s=0.30 f_y=450 MPa, r=0.002	k_ϕ=0.67	α_f=0°	p_i=0 MPa ΔT=0 °C	- ***Benchmark case*** - Effect of dip angle
2	*as case 1*				**p_i=8 MPa** ΔT=0 °C	Effect of ***internal gas pressure*** *alone*
3	*as case 1*				**p_i=8 MPa ΔT=50 °C**	Combined effect of ***internal gas pressure*** and ***temperature difference***
4	*as case 1 with* **G_{eq}=0.15G_{max}**	*as case 1*				Effect of ***soil elastic moduli***
5	**V_s=125 m/s, ρ=1.60 t/m^3** G_{eq}=0.33G_{max}, ν=0.25, **ϕ'=30°, ψ'=0°**, c'=0.1 kPa	*as case 1*	**k_ϕ=0.90**	*as case 1*		Effect of ***soil bearing pressure*** (with equal interface friction)
6	*as case 1*		**k_ϕ=1.00**	*as case 1*		Effect of ***interface friction*** (with equal soil bearing pressure)
7	*as case 1*			**α_f=45°**	**p_i=8 MPa ΔT=50 °C**	Effect of **fault crossing angle**

3.3. The benchmark case

To display the evolution of stress and strain throughout the pipeline as a function of the amplitude of fault offset, in Figure 7 the spatial variation of the Mises stress, normalized by the yield stress, is shown, together with the longitudinal strain computed along the upper and lower lines of the pipe for Δ_F = 0.4m – 0.8m – 1.5m.

Yielding is first attained in the FW side of the pipe along the upper line, for a fault offset slightly larger than 0.4 m, and, as Δ_F increases, yielding appears also on the HW side, along the lower line. In both cases, yielding occurs due to tensile stresses. At Δ_F = 1.5 m, yielding is largely diffused throughout a zone of about 50 m around the fault crossing, dominated by bending, which is represented in more detail by Figure 8. Note that, while on the FW side the plastic deformation is confined within a relatively narrow zone, roughly associated to the formation of a plastic hinge, yielding on the HW side is distributed along a much wider zone with Mises stress along the inner side of the pipe which hardly reach yielding also for Δ_F = 1.5 m. ~~Besides yielding, gradual evolution in plasticity and pipeline ovalization deformation were found quite reasonable, as well.~~ [RP: It is a rather vague statement: with no additional explanation, I suggest to take it out]

Another important result to point out for this initial case study, refers to the extension of the portion of the model affected by different deformation modes. As previously noted, a zone with predominant bending deformation appears across the fault intersection, with spatial extension $L_2 \approx$ 50m. Externally, both on the FW and HW sides, a region of prevailing longitudinal elongation appears, the extension of which, denoted by L_{1FW} and L_{1HW} (see sketch in Figure 9), is related to the amplitude of the fault offset. Although straining in this region provides a limited contribution to

the total deformation, the minimum longitudinal extension of the numerical model should include at least such elongation zones, in order to avoid any spurious effect on the results owing to numerical boundary conditions too close to the fault crossing. For this reason, we provide in Figure 10 quantitative evaluations of L_2, L_{1HW} and L_{1FW}. Results are also shown for the operating conditions, with internal gas pressure p_i=8MPa and temperature variation ΔT=50°C, which will be commented in more detail in the following section. From the left and mid panels of Figure 10, it can be deduced that the spatial extension of L_{1FW} and L_{1HW} is about the same, irrespective on the operating conditions, and it only depends on ΔF,x= ΔF$\cos\delta$, which is the projection of the fault offset along the pipe axis. As regards L_2, it is nearly independent on the magnitude of Δ_F, and roughly equals 50 m, where about 20% of such extension is on the FW side, where the largest plastic strains occur, while the remaining is on the HW side. Besides the benchmark value δ=80°, additional dip angles were considered (δ=90°, δ=60°, δ=40°). Relevant results are presented in the performance based framework in Table 2.

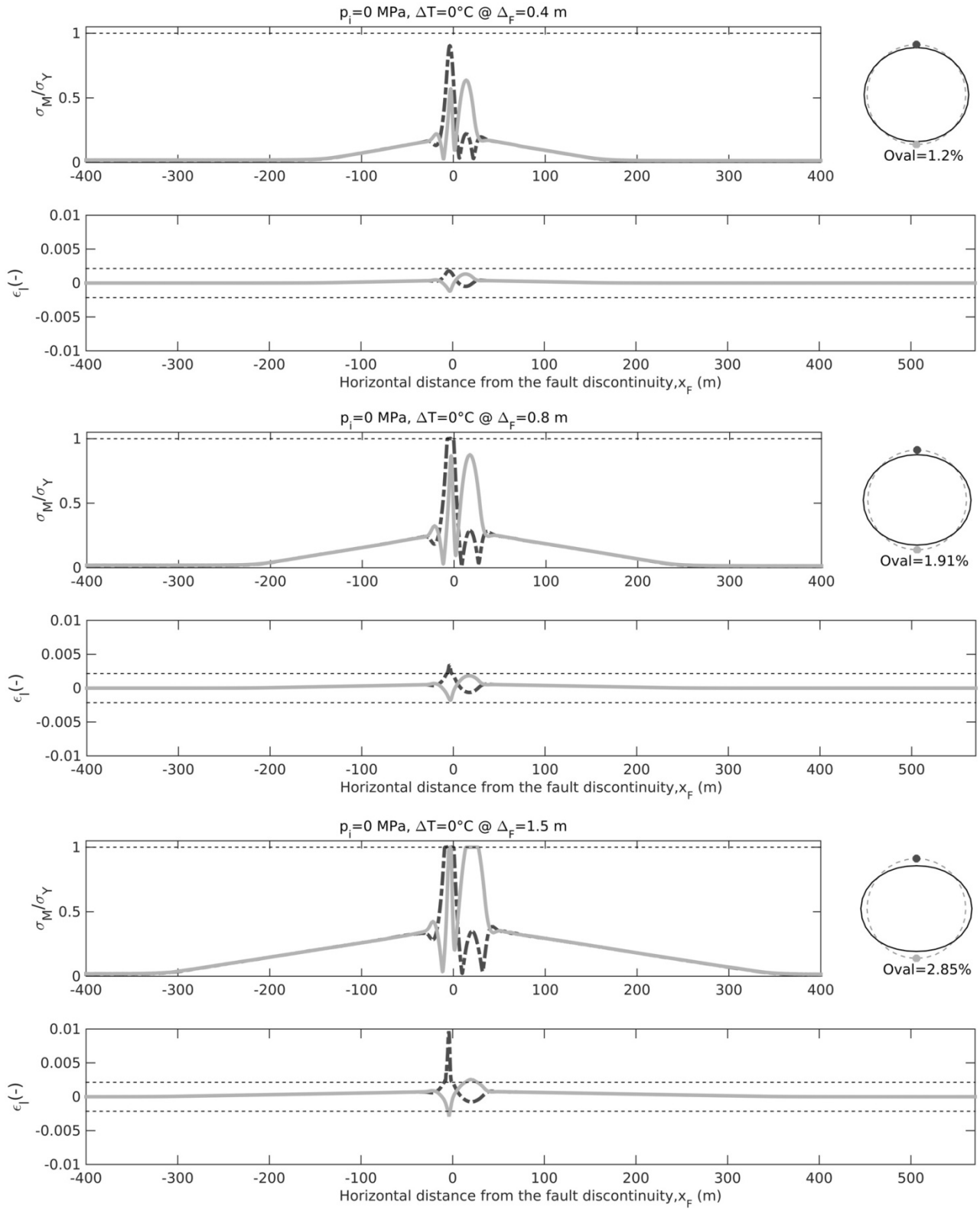

Figure 7. Case 1: Pipe response in terms of normalized Mises stress, longitudinal strain and cross-section ovalization (for the most-deformed cross-sections on footwall region). Fault offsets 0.4 (top), 0.8 (middle) and 1.5 m (bottom). The values for the upper line of the pipe (thick dashed), and for the lower line (thin gray) are shown. The undeformed (dashed line) and deformed (continuous line) cross-sections are also illustrated.

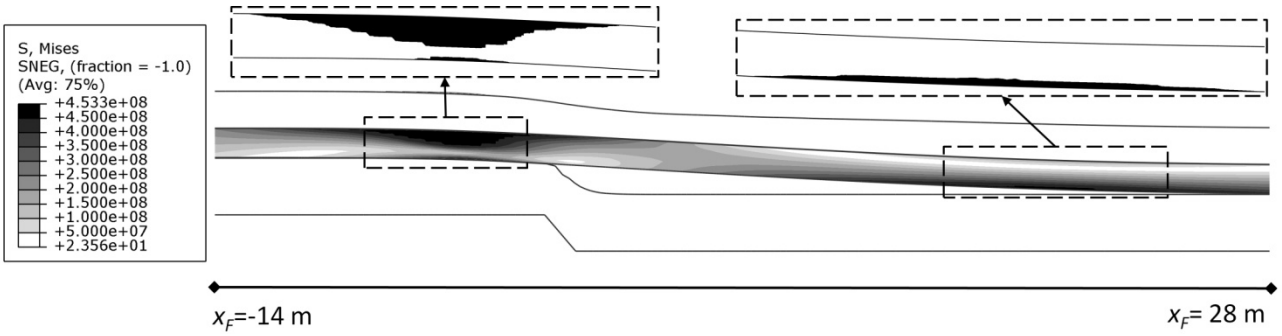

Figure 8. Case 1: deformed configuration of the pipe for fault offset 1.5 m in the vicinity of the fault crossing, with identification of the Mises stress distribution. In zoom-up windows, the plastic equivalent strains are indicated (black color: PEEQ > 10^{-5})

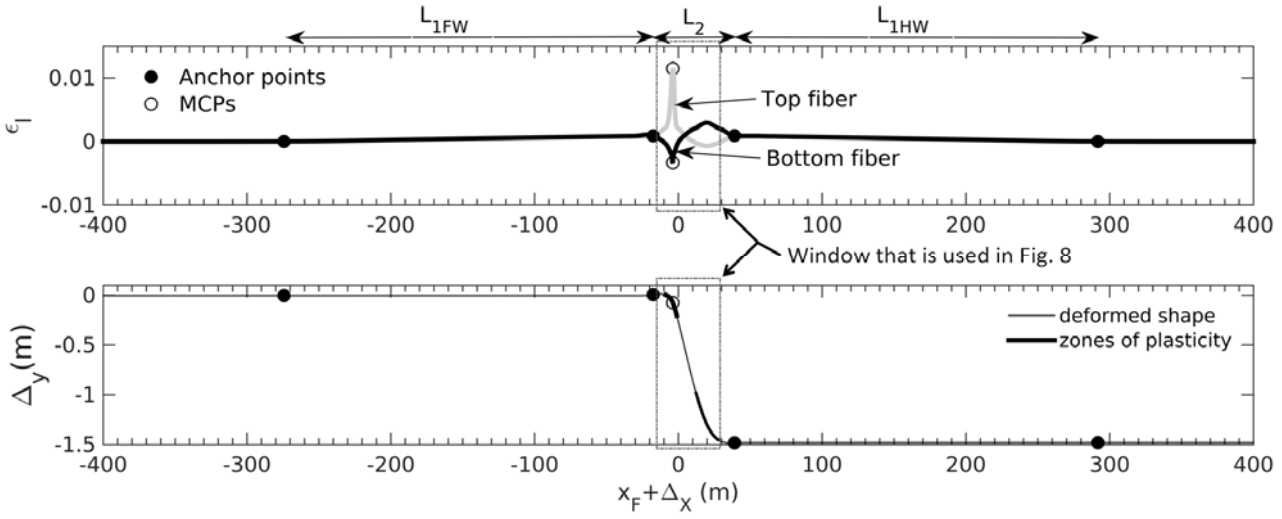

Figure 9. Case 1: deformed configuration of the pipe for fault offset 1.5 m, and identification of the main deformation zones. L_{1FW} and L_{1HW}: length of the pipe trunk subject to tensional, along the foot (FW) and hanging wall (HW), respectively. L_2: length of the pipe trunk subject to combined tension and bending. Panel denotes the zoomed area illustrated in Fig. 8. MCPs: Maximum curvature points.

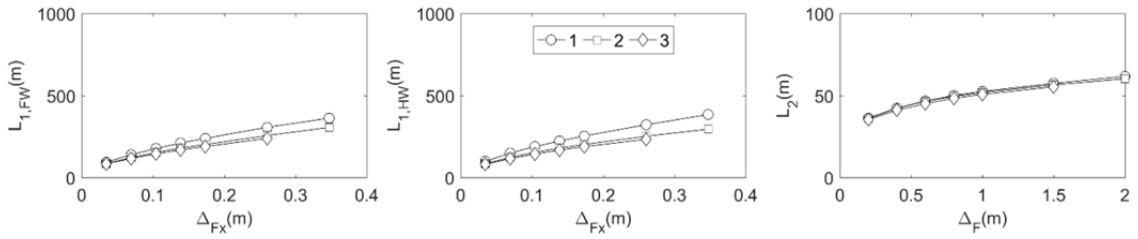

Figure 10. Effect of dip angle on the deformation features (see Fig. 9) of the pipeline, for Cases 1 (pi=0, ΔT=0), 2 (pi=8 MPa, ΔT=0) and 3: pi=8 MPa, ΔT=50°C. Note, from the left and middle panels, that the length of the pipeline trunk in tension is about the same for the FW and HW sides and depends on $\Delta F,x= \Delta F\cos\delta$, which is the projection of the fault offset along the pipe axis. On the right side, it is shown that the length of the pipe trunk mainly subject to combined tension and bending (L_2) has only a moderate dependence on ΔF, and its value is around 50 m.

3.4. Impact of operating conditions

We now focus on the variation of the solution when operating conditions are also considered in addition to the fault offset loading. A similar investigation was also reported in [28]. We started from considering the internal gas pressure alone (Case 2, p_i=8MPa) and subsequently a temperature variation ΔT=50°C was also introduced (Case 3). In Figure 11, the stress ratio (σ_M/σ_Y) and the corresponding longitudinal strain (ε_l) observed in the extreme top and extreme bottom fibers are shown, for the single case of fault offset Δ_F=1.5m. In addition, the cross-section ovalization is also shown.

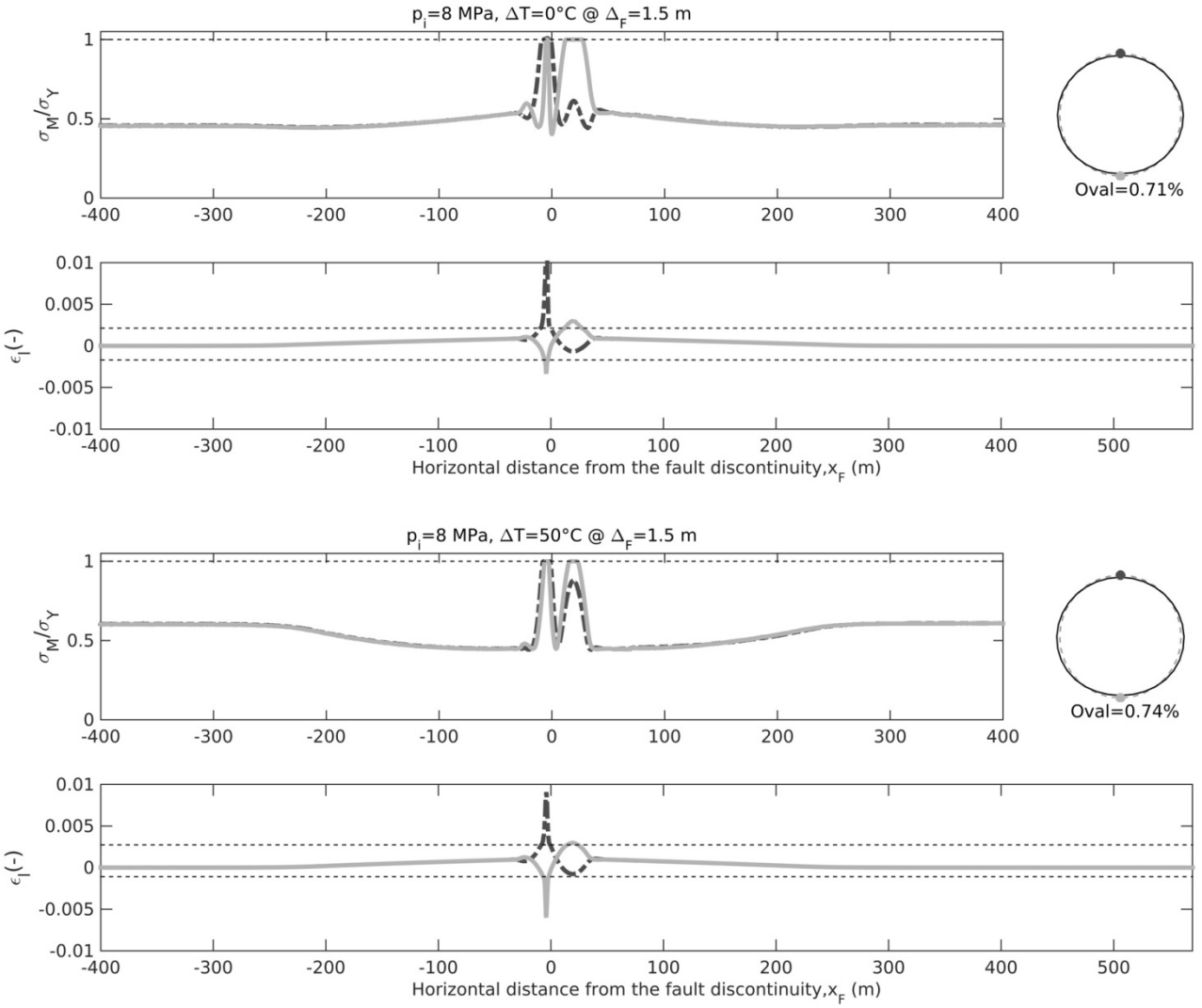

Figure 11. Stress ratio (σ_M/σ_Y), longitudinal strain (ε_l) and cross-section ovalization (for the most-deformed cross-section on footwall plastic hinge region). for Case 2 (top, p_i=8MPa, ΔT=0) and Case 3 (bottom, p_i=8MPa, ΔT=50°C) for the fault offset Δ_F = 1.5 m (bottom). Dashed lines indicate the values at yielding.

If we compare Figure 11 with the corresponding profiles for Case 1, illustrated at the bottom of Figure 7, some important remarks can be made:

- Owing to the effect of p_i, cross-sectional ovalization is significantly reduced from about 3% in Case 1, to about 0.7% in both Cases 2 and 3;
- Due to the initial operating conditions, straining due to the fault offset is larger, both in tension and compression, with significant, albeit localized, plastic hinging on the FW side, but also with a more widespread plastic zone along the HW side. The Mises stress pattern for Case 3 is illustrated in Figure 12.
- The length of the plastic hinge along the FW side extends significantly, up to about 7 times the pipe diameter. To clarify this result, we illustrate in Figure 13 the evolution of the extent of the plastic zone in tension and compression, as a function of the fault offset and of the operating

conditions. It appears that consideration of ΔT has a major impact on the length of plastic zone in compression, which becomes almost as wide as the plastic zone in tension, while in the other cases plastic hinge length is dominated by tension.

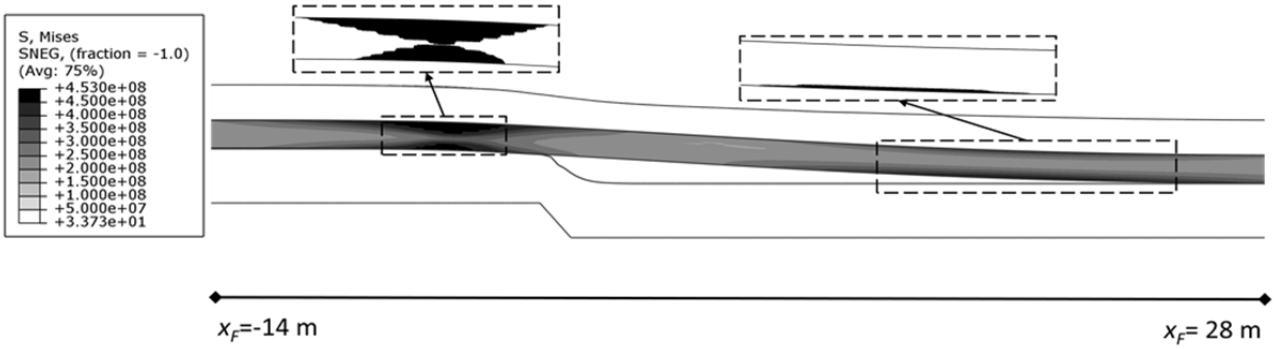

Figure 12. Case 3 (combined effect of p and ΔT) : deformed configuration of the pipe for fault offset 1.5 m, with identification of Mises stress (black colour indicates yielding). In zoom-up windows, PEEQ distributions are shown (black color: PEEQ > 10^{-5}).

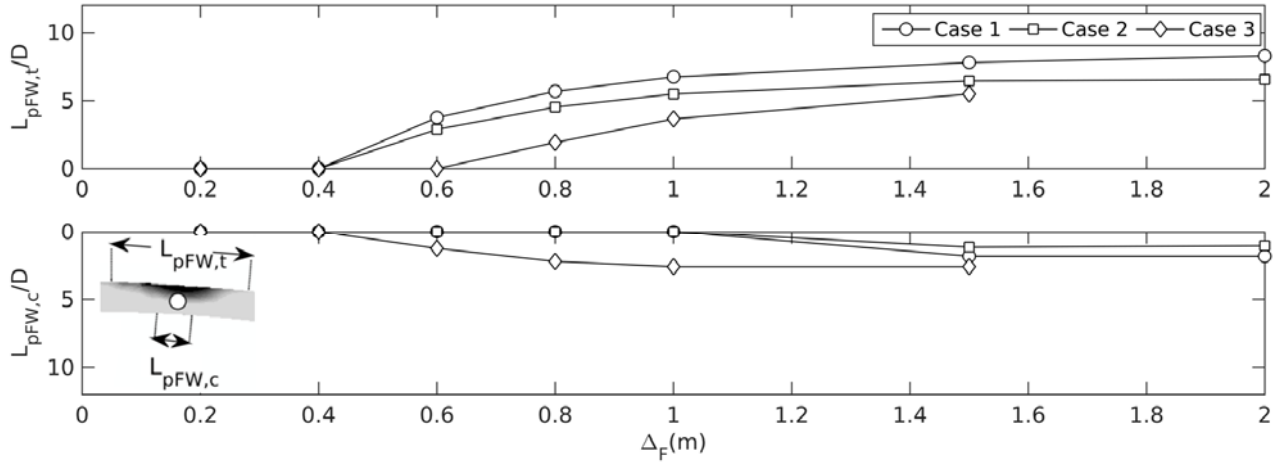

Figure 13. Length of plastic zone in tension ($L_{pFW,t}$) and compression ($L_{pFW,c}$) of the most deformed portion of the pipeline along the FW. Values are normalized by the pipe diameter D. Different operating conditions (Cases 1, 2, 3) are considered.

3.5. Pipeline performance

The pipeline performance for increasing fault offsets was verified based on the following criteria, by making reference to Part 4 of Eurocode 8 [5]:

Damage limit state (DLS):

$$\varepsilon_{t,y} = \varepsilon_{c,y} = 0.002 \quad (1a)$$

Ultimate limit state (ULS):

$$\varepsilon_{t,u} = 0.03 \quad (1b)$$

$$\varepsilon_{c,u} = \min\left(-0.01, -0.4t/D\right) \quad (1c)$$

where, in eq. 1a, $\varepsilon_{t,y}$ and $\varepsilon_{c,y}$ are the yield longitudinal strains, while in eq. 1b and 1c $\varepsilon_{t,u}$ and $\varepsilon_{c,u}$ are the ULS strains in tension and compression, respectively, t represents the cross-sectional thickness and D is the pipe diameter. Owing to the distance between DLS and ULS performance levels, an intermediate damage threshold limit state (ILS) was also considered, represented by a strain value 0.5%.

Following ALA Guidelines [2], we also addressed the limit for ovalization deformation (ranging from 2% to 5%), but, according to results shown previously, this is not a matter for operating conditions because of the positive effect of internal gas pressure.

Performance checks are shown in Figure 14 for Cases 1, 2 and 3, referring to the fault dip angle δ=80°. It is found that yielding first occurs in compression in Case 3, for a fault offset of about 40 cm (see bottom panel in Figure 14). This is a somehow surprising result, because a pipeline under normal faulting is expected to be mostly subjected to tensile straining. However, the presence of a high variation of temperature (ΔT=50°C) induces a significant compressive pre-stress which adds to the compressive bending stresses along the FW side of the pipe when fault offset occurs.

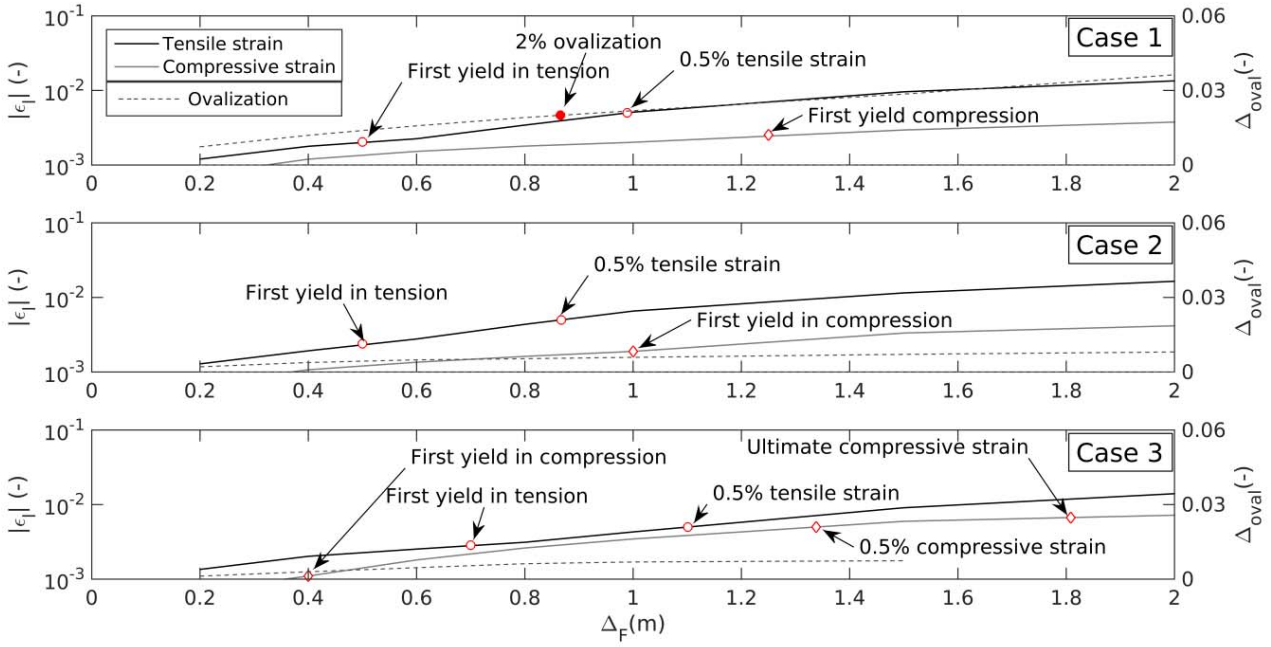

Figure 14. Pipeline performance measured, as a function of fault offset, in terms of longitudinal strain in tension (thick continuous line), longitudinal strain in compression (thin continuous line), cross-sectional ovalization. From top to bottom: Case 1, Case 2, Case 3. Attainment of a limit state is denoted by an arrow.

3.6. Effect of non-perpendicular fault crossing

Since the orientation of the fault rupture plane may be subjected to large uncertainties, also because of the complicated patterns based on which the fault rupture may propagate through the shallow ground surface layers, it is interesting to determine the sensitivity of the solution to the fault plane orientation, which, up to now, was considered to have a unit normal vector directed as the longitudinal axis of the pipe (α_f = 0°, as in Figure 15). A thorough sensitivity study implies a large computational effort and it is beyond the scope of this paper. However, to start shading light on this subject and to point out its practical relevance, we have considered a single case study, obtained based on Case 3 (δ=80°, p_i=8 MPa, ΔT=50°C), but with a normal vector forming an angle α_f = 45° with the longitudinal axis of the pipe, as sketched representatively in Figure 15.

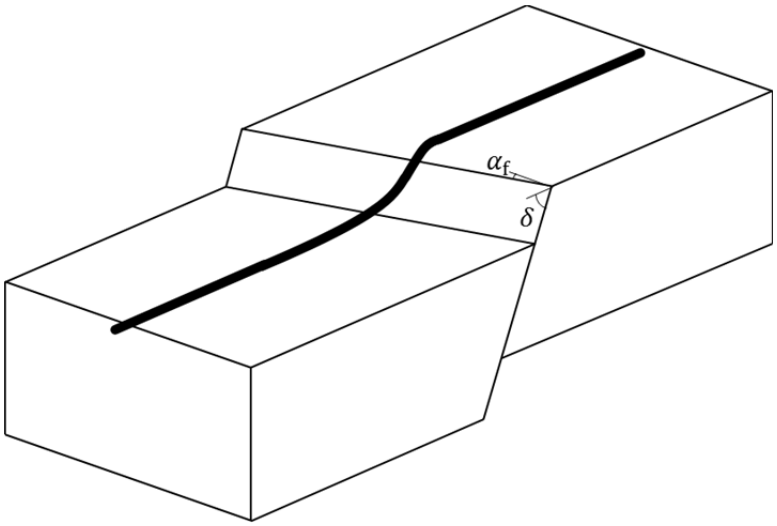

Figure 15. Sketch of the case of non-perpendicular normal fault-crossing

The non-perpendicular fault-crossing condition turns out to be more severe, with all limit states reached in compression, and limit fault offsets of about 0.2-0.3 m for DLS (against 0.3-0.4 m for the perpendicular case), 0.6-0.7 m for ILS (against 1.0-1.25 m, reached in tension for the perpendicular case), and 0.8 m for ULS (against 1.5-1.75 m) (see Table 2, Case III vs Case IX). To clarify reasons of such result, in Figure 16 the longitudinal strain distribution is plotted along the upper and lower generatrixes of the pipe, for the case of a fault offset ΔF =1.0 m and α_f=45°. Furthermore, the polar distribution of the longitudinal strain in the most heavily loaded cross-sections on the FW and HW sides of the pipe are shown.

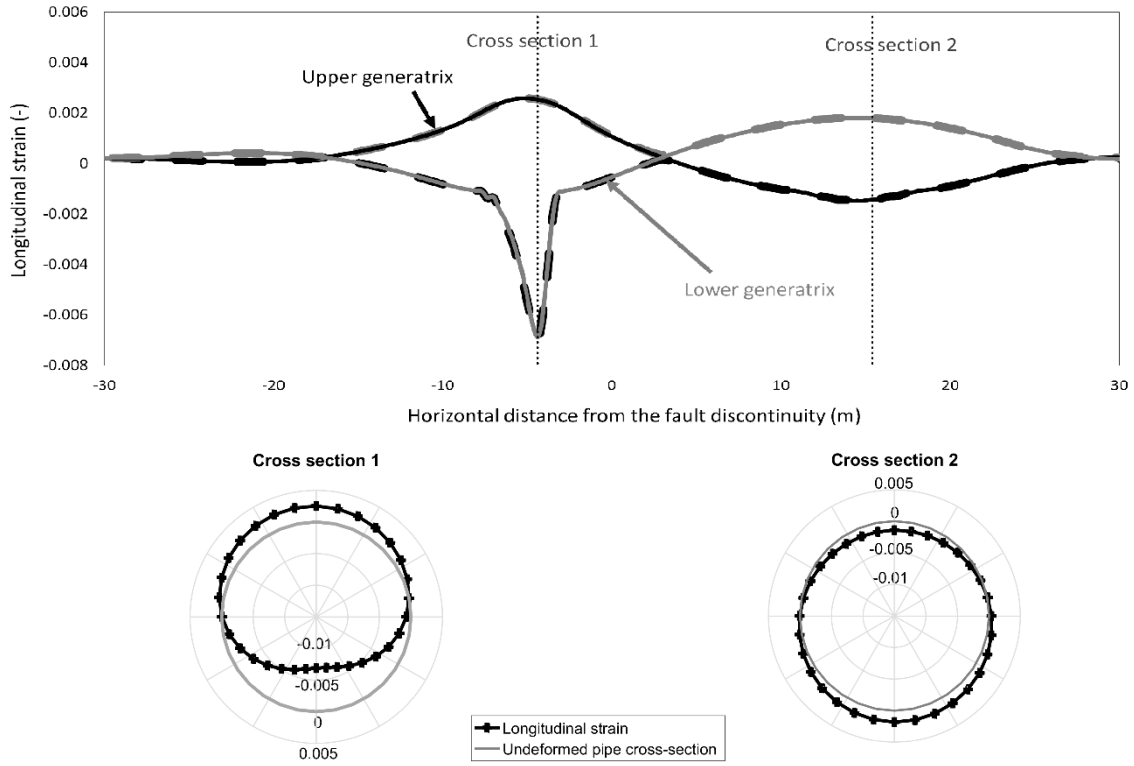

Figure 16. Top: Envelope of the maximum longitudinal strain distribution along the upper and lower generatrixes of the pipe. Bottom: Polar plots of the longitudinal strain across the most heavily loaded cross-sections on the FW (left) and HW (right) sides of the pipe.

It turns out that the pipe in the non-perpendicular case is negatively affected by the following main factors: (a) given the same normal fault offset, the elongation component is reduced and the bending component increased, with a consequent increase of the compressive strain in the most critical cross-section of the FW trunk; (b) mobilization of passive soil pressure at the lateral side induces a further constrain which tends to increase bending of the pipe, which reaches yielding also within the HW trunk.

Although this is a preliminary result, which deserves further investigations and numerical simulations, it should be pointed out that the common assumption of disregarding the non-perpendicular components of normal faulting may lead to unconservative results. This is especially true for those cases, like the pressurized pipe subject to temperature variation considered in this study, where the limit state of the pipe in the perpendicular fault-crossing is reached in compression. When the limit state is reached in tension, then the non-perpendicular fault crossing may improve performance, but only until compressive strains become predominant.

3.7 Parametric study

A parametric summary of results for the different cases considered in this study is reported in Table 2, in terms of fault offset value ΔF required to reach a given performance level. The following indications may be drawn.

- In general, normal fault crossings create tensile plastic deformations. However, in the case of operating temperature variation, compressive strains may be significant, especially for high dip angles, and govern the attainment of performance limit state.
- The internal pressure~~, itself,~~ does not significantly affect performance in terms of strain limits (see case 2 vs case 1). However, the ovalization performance is significantly enhanced.
- The increase of operating temperature variation makes the system slightly more resilient in terms of tensile deformation and significantly more vulnerable in terms of compressive deformation (see case 3 vs case 1). Since it is usually coupled with internal pressure, the ovalization performance is enhanced.
- Decrease in dip angle (Cases 1 to 6) does not significantly change the performance in tension. It significantly improves the performance of the pipe against compressive failure. Ovalization performance is inversely influenced.
- Increase of bearing pressure and elastic stiffness (Cases 4 and 5 vs case 1) slightly decreases the performance of the pipe in terms of tensile, compressive, and ovalization deformations.
- Increase of interface strength (Case 6 vs Case 1) significantly reduces the performance in terms of tension. The reverse happens in terms of compressive strains. Since tearing off is the likely failure mechanism, cross sectional deformations are also increased.
- Fault offsets to reach the DLS are compared (see values in parentheses for case 1 in Table 2) with those computed by the simplified analytical method proposed by Karamitros et al. [13], showing a reasonably good agreement.
- For a dip angle δ=90°, which was considered only for Case 1, an abrupt reduction of the fault offset to reach the ULS is found, consistent with the vanishing contribution of the fault offset elongation component along the pipe axis. Moreover, governing mechanism of the pipeline is shifted to compressional type in all performance levels. Although this case is of limited practical relevance, since no normal faults is expected along a vertical plane, it points out the relevance of the elongation component of the fauls offset in the overall good performance of the pipeline subjected to normal faulting.
- Finally, it is important to note that non-perpendicular normal fault crossing (Case 7 vs Case 1) decreases performance in terms of compressive straining and improves in terms of tensile straining. Ovalization deformations were not investigated for non-perpendicular normal fault crossing case.

Table 2. Values of fault offset (in m) associated to the exceedance of limit states defined for the case studied. Damage limit state (DLS, ε=0.2%); intermediate damage limit state (ILS, ε=0.5%); ultimate limit state (ULS, eqs. 1b and 1c)); ovalization (OLS). Attainment of the limit state in compression or in tension is denoted by C or T, respectively. The values in parantheses are the fault offset values at first yield obtained by using the simplified analytical procedure of Karamitros et al. [13], which are noted as their first exceedances for each 10 cm increase in the fault offset.

	DLS		**ILS**		**ULS**		**OLS**	
	Δ_F(m)	**T/C**	**Δ_F(m)**	**T/C**	**Δ_F (m)**	**T/C**	**2%**	**5%**
Case 1-δ=80°	0.4-0.5 (0.6)	T	0.9-1.0	T	> 2	-	0.8-0.9	> 2
Case 1-δ=90°	0.5-0.6	C	0.9-1.0	C	1.0-1.1	C	0.8-0.9	> 2
Case 2-δ=80°	0.4-0.5	T	0.8-0.9	T	> 2	-	> 2	> 2
Case 3-δ=80°	0.3-0.4	C	1.0-1.25	T	1.5-1.75	C	> 1.75	> 1.75
Case 4-δ=80°	0.5-0.6	T	1.0-1.25	T	> 2	-	1.0-1.25	> 2
Case 5-δ=80°	0.6-0.7	T	1.0-1.25	T	> 2	-	1.5-1.75	> 2
Case 6-δ=80°	0.3-0.4	T	0.7-0.8	T	> 2	-	0.8-0.9	> 2
Case 1-δ=60°	0.4-0.5 (0.5)	T	0.9-1.0	T	> 2	-	1.25-1.5	> 2
Case 2-δ=60°	0.4-0.5	T	0.8-0.9	T	> 2	-	> 2	> 2
Case 3-δ=60°	0.6-0.7	T	1.0-1.25	T	> 2	-	> 2	> 2
Case 4-δ=60°	0.5-0.6	T	1.0-1.25	T	> 2	-	1.5-1.75	> 2
Case 5-δ=60°	0.6-0.7	T	1.25-1.5	T	> 2	-	> 2	> 2
Case 6-δ=60°	0.3-0.4	T	0.5-0.6	T	1.25-1.50	T	1.0-1.25	1.25-1.5
Case 1-δ=40°	0.5-0.6 (0.5)	T	1.0-1.25	T	> 2	-	1.75-2.0	> 2
Case 2-δ=40°	0.4-0.5	T	0.8-0.9	T	> 2	-	> 2	> 2
Case 3-δ=40°	0.7-0.8	T	1.0-1.25	T	> 2	-	> 2	> 2
Case 4-δ=40°	0.5-0.6	T	1.0-1.25	T	> 2	-	1.75-2.0	> 2
Case 5-δ=40°	0.6-0.7	T	1.25-1.5	T	> 2	-	> 2	> 2
Case 6-δ=40°	0.3-0.4	T	0.5-0.6	T	0.8-0.9	T	0.7-0.8	> 0.9
Case 7-δ=80°	0.2-0.3	C	0.6-0.7	C	0.8-0.9	C	> 0.9	> 0.9

4. CONCLUSIONS

In this paper we investigated from a numerical point of view the performance levels of a gas pipeline subjected to normal fault rupture, for increasing values of the fault offset and considering also the influence of the operating conditions, including the effect of internal gas pressure and variation of temperature.

After providing some practical guidelines to properly select the spatial extension of the numerical model in the longitudinal direction, in order to reduce the effect of boundary conditions on the numerical results, we carried out a set of 3D nonlinear numerical simulations, useful to clarify the response of the pipeline up to extreme loading conditions, with fault offset up to 2 m, which is usually considered as an upper threshold in the case of normal faulting.

It was found that pipeline initially yields (DLS) for values of fault offset of about 0.3 to 0.5 m, with worst conditions occurring in the case of high values of the friction angle at the pipeline-soil interface, or for large temperature gradients, typically increasing compression stress throughout the pipeline. For increasing values of the fault offset, the ultimate limit state (ULS), defined as in the Eurocode 8 Part 4 in terms of a 3% longitudinal strain in tension and ultimate limit in compression, is reached only in few cases, typically related to high interface friction angles and low values of the fault dip angle.

While this in general confirms the good performance of pipelines under normal faulting, mainly because of prevailing tensional stresses, so that, in presence of sufficiently loose soils in the pipe trench, the fault offset may exceed in most cases 2 m without reaching the ULS, an important outcome of this research work is the sensitivity of the solution to the case of non-perpendicular fault-crossing, i.e., when the normal to the fault plane is not contained in the longitudinal plane of the pipe. Contrary to the expectations, the non-perpendicular crossing case turned out to be more severe, with all limit states reached in compression, and limit fault offsets of about 0.2-0.3 m for DLS and 0.8 m for ULS, in the case α_F=45°. This was argued to be related to the mobilization of passive soil pressure at the lateral side of the pipe effect, with an increase of the bending component of deformation, and a corresponding increase of the compressive strain in the most critical cross-sections of the pipeline.

Acknowledgements

Authors are grateful to two anonymous reviewers, the comments of which contributed to improve the clarity of the paper.

5. REFERENCES

[1] Abdoun TH, Ha D, O'Rourke MJ, Symans MD, O'Rourke T, Palmer MC, Stewart HE (2009). Factors influencing the behavior of buried pipelines subjected to earthquake faulting. Soil Dynamics and Earthquake Engineering, 29: 415-427, doi: 10.1016/j.soildyn.2008.04.006.

[2] ALA (2001). Guidelines for the design of buried steel pipe. American Lifelines Alliance, website: www.americanlifelinealliance.org, July 2001, 76 pp.

[3] ASCE (1984). Guidelines for the seismic design of oil and gas pipeline systems. Prepared by the ASCE Technical Council on Lifeline Earthquake Engineering, D.Nyman Principal Investigator.

[4] Bransby MF, Davies MCR, El Nahas A (2008). Centrifuge modeling of normal fault-foundation interaction. Bulletin of Earthquake Engineering, 6: 585-605.

[5] CEN, European Committee for Standardization (2006). Eurocode 8 – Design of structures for earthquake resistance, Part 4: Silos, tanks and pipelines. Final draft, January 2006, prEN 1998-4.

[6] Dassault Systèmes (2013). Abaqus 6.13. Finite element code and the documentation.

[7] Datta TK (1999). Seismic response of buried pipelines: a state-of-the-art review. Nuclear Engineering and Design, 192: 271-284.

[8] Eidinger JM, O'Rourke MJ, Bachhuber J (2002). Performance of a pipeline under large fault displacement. In Proceedings of 7th U.S. National Conference on Earthquake Engineering, Oakland, California.

[9] Ha D, Abdoun TH, O'Rourke MJ, Symans MD, O'Rourke TD, Palmer MC, Stewart HE (2008). Buried high-density polyethylene pipelines subjected to normal and strike-slip faulting – a centrifuge investigation. Canadian Geotechnical Journal, 45: 1733-1742.

[10] Hall W and Newmark N (1977). Seismic design criteria for pipelines and facilities. In Proceedings of Technical Council of Lifeline Earthquake Engineering Specialty Conference, 31 August 1977, Los Angeles, ASCE NY: 18-34.

[11] Joshi S, Prashant A, Arghya D, Jain SK (2011). Analysis of buried pipelines subjected to reverse fault motion. Soil Dynamics and Earthquake Engineering, 31: 930-940.

[12] Karamitros DK, Bouckovalas GD, Kouretzis GP (2007). Stress analysis of buried pipelines at strike-slip fault crossings. Soil Dynamics and Earthquake Engineering, 27: 200-211.

[13] Karamitros DK, Bouckovalas GD, Kouretzis GP, Gkesouli V (2011). An analytical method for strength verification of buried pipelines at normal fault crossings. Soil Dynamics and Earthquake Engineering, 31: 1452-1464.

[14] Kennedy RP, Chow AW, Williamson (1977). Fault movement effects on buried oil pipeline. Journal of Transpor. Eng. Division-ASCE, 103(TE5): 617-633.

[15] Liu X, Zhang H, Li M, Xia M, Zheng W, Wu K, Han Y (2016). Effects of steel properties on the local buckling response of high strength pipelines subjected to reverse faulting. Journal of Natural Gas Science and Engineering, 33: 378-387.

[16] Miyajima, M. and Hashimoto, T. (2001), "Damage to water supply system and surface rupture due to fault movement during the 1999 Ji-Ji earthquake in Taiwan", Proc. 4th Int. Conf. Rec. Adv. in Geotechnical Earthq. Eng. and Soil Dyn., San Diego, CA, Paper 10.45.

[17] Moradi M, Rohjani M, Galandarzadeh A, Takada S (2013). Centrifuge modeling of buried continuous pipelines subjected to normal faulting. Earthquake Engineering and Engineering Vibration, 12(1): 155-164, doi: 10.1007/s11803-013-0159-z.

[18] Newmark NM and Hall WJ (1975). Pipeline design to resist large fault displacement. In Proceedings of U.S. National Conference on Earthquake Engineering, Ann Arbor, Michigan: 416-425.

[19] O'Rourke TD and Palmer MC (1994). Earthquake performance of gas transmission pipelines. In Proceedings of the Fifth U.S.-Japan Workshop on Earthquake Resistant Design of Lifeline Facilities and Countermeasures Against Soil Liquefaction, Snowbird, Utah. Technical Report NCEER-94-0026, Multidisciplinary Center for Earthquake Engineering Research (MCEER), A National Center of Excellence in Advanced Technology Applications, Buffalo, New York: 679-702.

[20] O'Rourke MJ and Liu X (1999). Response of buried pipelines subject to earthquake effects. Monograph Series. Multidisciplinary Center for Earthquake Engineering Research (MCEER), A National Center of Excellence in Advanced Technology Applications, Buffalo, New York, 249 pp.

[21] Özcebe AG, Paolucci R, Mariani S, Santoro D (2015). A numerical study of the pressurized gas pipeline-normal fault interaction problem. In Proceedings of 6th International Conference on Earthquake Geotechnical Engineering, 1-4 November 2015, Christchurch, New Zealand.

[22] Paolucci R, Griffini S, Mariani S (2010). Simplified modeling of continuous buried pipelines subject to earthquake fault rupture. Earthquakes and Structures, 1(3): 253-267, doi: 10.12989/eas2010.1.3.253.

[23] Rohjani M, Moradi M, Galandarzadeh A, Takada S (2012). Centrifuge modeling of buried continuous pipelines subjected to reverse faulting, Canadian Geotechnical Journal, 49: 659-670, doi: 10.1139/T2012-022.

[24] Sim WW, Towhata I, Yamada S, Moinet GJ-M (2012). Shaking table tests modeling small diameter pipes crossing a vertical fault. Soil Dynamics and Earthquake Engineering, 35: 59-71.

[25] Tarinejad R, Mahdavi A, Jahangir N (2012). Buried pipeline response analysis to reverse-slip fault displacements. 15th World Conference on Earthquake Engineering, Lisbon (Portugal).

[26] Trifonov OV (2015). Numerical stress-strain analysis of buried steel pipelines crossing active strike-slip faults with an emphasis on fault modeling aspects. Journal of Pipeline Systems Engineering and Practice, 6 (1).

[27] Trifonov OV and Cherniy VP (2010). A semi-analytical approach to a nonlinear stress-strain analysis of buried steel pipelines crossing active faults. Soil Dynamics and Earthquake Engineering, 30: 1298-1308.

[28] Trifonov OV and Cherniy VP (2012). Elastoplastic stress-strain analysis of buried steel pipelines subjected to fault displacements with account for service loads. Soil Dynamics and Earthquake Engineering, 33: 54-62.

[29] Wang LRL and Yeh Y (1985). A refined seismic analysis and design of buried pipeline for fault movement. Earthquake Engineering and Structural Dynamics, 13: 75-96.

[30] Wells DL, Coppersmith KJ (1994). New empirical relationships among magnitude, rupture length, rupture width, rupture area, and surface displacement. Bulletin of Seismological Society of America, 84(4): 974-1002.

[31] Xie X, Symans MD, O'Rourke MJ, Abdoun TH, O'Rourke TD, Palmer MC, Stewart HE (2011). Numerical modeling of buried HDPE pipelines subjected to strike-slip faulting. Journal of Earthquake Engineering, 15(8): 1273-1296, doi: 10.1080/13632469.2011.569052.

[32] Xie X, Symans MD, O'Rourke MJ, Abdoun TH, O'Rourke TD, Palmer MC, Stewart HE (2013). Numerical modeling of buried HDPE pipelines subjected to normal faulting: a case study. Earthquake Spectra, 29(2): 609-632, doi: 10.1193/1.4000137.

[33] Vazouras P, Karamanos SA, Dakoulas P (2012). Mechanical behavior of buried steel pipes crossing active strike-slip faults. Soil Dynamics and Earthquake Engineering, 41: 164-180.

[34] Vazouras P, Dakoulas P, Karamanos SA (2015). Pipe-soil interaction and pipeline performance under strike-slip fault movements. Soil Dynamics and Earthquake Engineering, 72: 48-65.